IEEE Open Journal of Vehicular Technology

Received 8 December 2022; accepted 29 December 2022. Date of publication 4 January 2023;
date of current version 27 January 2023. The review of this article was coordinated by Editor Chenhao Qi.

Digital Object Identifier 10.1109/OJVT.2022.3233857

IRS-Assisted Full Duplex Systems Over Rician and Nakagami Fading Channels

SUYUE LI [1], SEN YAN [1], LINA BARIAH [2] (Senior Member, IEEE), SAMI MUHAIDAT [2,3] (Senior Member, IEEE), AND ANHONG WANG [1]

[1]School of Electronic and Information Engineering, Taiyuan University of Science and Technology, Taiyuan 030024, China
[2]KU Center for Cyber-Physical Systems, Khalifa University, Abu Dhabi, UAE
[3]Department of Systems and Computer Engineering, Carleton University, Ottawa, ON K1S 5B6, Canada

CORRESPONDING AUTHOR: SUYUE LI (e-mail: sy_li@126.com)

This work was supported in part by General Program of Shanxi Province Basic Research under Grant 20210302123205, in part by Shanxi Scholarship Council of China through Research Project under Grant 2022-162, in part by TYUST Innovative Projects in Graduate Education under Grant SY2022024, and in part by National Natural Science Foundation of China under Grants 61501315, 62071294, and 62072325.

ABSTRACT Intelligent reflecting surface (IRS) has been deemed as an energy and spectral-efficient technology, that can potentially enhance network coverage and transmission reliability, with minimum impact on transceivers' complexity. Motivated by this, we develop a comprehensive analysis on the performance of integrating IRS into full-duplex (FD) cellular or Internet of Things (IoT) networks in both realistic Rician and Nakagami fadings. Firstly, in the context of reciprocal channels in Rician fadings, we derive the closed-form approximations of the users' outage probability (OP) and ergodic capacity (EC), under the non-central Chi-square distribution assumption on the signal-to-interference-plus-noise ratio (SINR). Further following by the Gamma distribution assumption on the SINR, we derive the cumulative distribution function (CDF) expression of the user's SINR, which is then leveraged to obtain simple yet effective closed-form expressions in terms of OP and EC. Subsequently, in Nakagami fading scenarios with the reciprocal and non-reciprocal channels, the closed forms of both users' OP and EC are obtained. Finally, the correctness of all the theoretical expressions is verified through substantial Monte Carlo simulations. The results indicate that the OP and EC deduced from Gamma distribution exhibit the fairly precise results for the arbitrary number of IRS elements, especially in Nakagami fadings.

INDEX TERMS Full-duplex, intelligent reflecting surfaces, non-reciprocal, reciprocal, Rician and Nakagami fadings.

I. INTRODUCTION

Due to the technological breakthroughs in the fields of programmable metamaterials and microelectromechanical systems, intelligent reflective surface (IRS) emerges as a prominent solution for improving the spectrum and energy efficiency of mobile networks, as well as enhancing the quality of wireless links in beyond 5G networks [1]. Thanks to the passive elements of the IRS, thermal noise and self-interference have a negligible effect on the wireless signals. Generally speaking, IRS has been shown to be superior to conventional active decode/amplify-and-forward relays in the aspects of transmission rate and energy efficiency [2]. IRS consists of a large number of reflective elements, which can be passive or active, ultra-low power elements, each of which can independently apply a continuous or discrete adjustable phase shifts to the incident signal [3], [4]. Besides, despite the experienced self-interference (SI), a two-user full duplex (FD) communication system allows users to simultaneously send and receive information over the same channel, rendering it a spectrally efficient mechanism [5], [6]. Therefore, it is anticipated that the integration of IRS into FD systems will bring up additional benefits in terms of spectrum and energy efficiencies.

Motivated by the potential advantages of IRSs, the integration of IRS into diverse key technologies, for instance, deep learning [7], [8], wireless energy transfer [9], non-orthogonal multiple access (NOMA) [10], to name a few, has been thoroughly explored in the past two years.

Specifically, the particular attention was devoted for the performance analysis and system optimization of IRS-aided wireless communications, under the Rayleigh [11], [12] and Rician fading channels [13], [14], [15]. [13] provided the asymptotic expressions for the upper bound on channel capacity, as well as outage probability (OP), while the Rician fading was considered over the IRS links, with the direct-link channel modeled as Rayleigh fading. In [14], the cascaded channel is modelled as a non-central chi-square distribution, and upper bounds on the bit error ratio (BER) are offered for single and multiple IRS-assisted communication systems involving indoor and outdoor, under the assumption of a blocked direct link. The authors in [15] investigated the accurate closed-form expressions of some performance metrics such as OP, channel capacity, as well as average symbol error probability (SEP) in the Rician fading. Considering the fluctuating two-ray distribution of millimetre wave frequencies, Du et al. [16] derived the OP and the average BER for IRS systems. Additionally, the performance of IRS-enabled wireless systems is studied over Nakagami fading in [17], [18], [19], [20]. Selimis et al. [17] analyzed the outage probability and ergodic capacity, taking random and coherent phase shift configurations into account. The OP and energy efficiency (EE) are investigated in both overlay device-to-device (D2D) and underlying D2D modes in [18]. The integration of IRS into NOMA systems is presented in [19], [20], with [19] analyzing the outage performance in an IRS-assisted NOMA downlink system, and [20] investigating the outage performance for the uplink scenario.

On the other hand, although it is still in its early stages, there are numerous studies presented in order to improve the performance when IRS is utilized in FD wireless networks. The authors in [21] derived the OP and the average SEP in an IRS-assisted FD wireless communication system with Nakagami fading environment. In [22], Lu and Wang focused on the OP for an arbitrary IRS reflecting coefficient in an IRS-aided two-way FD system, over correlated Rayleigh fading. Atapattu et al. [23] addressed the outage performance and spectral efficiency analyses for IRS-assisted two-way communication systems over Rayleigh fading channels. Apart from these, other literature relevant to IRS/RIS FD is summarized in Table 1, where the complex Gaussian (denoted as $\mathcal{CN}$) assumptions are basically made about residual self-interference (RSI) or hardware impairment (HI). It is also noted that user, access point (AP) or relay can be in FD mode, allowing one or more FD nodes to coexist with other half-duplex(HD) nodes. Generally, one-way FD decode-and-forward (DF) relay is available for cooperative IRS/RIS FD systems [24], [25]. The papers [26], [27], [28], [30] addressing two-way FD primarily focus on the reciprocal channel which facilitates the received energy maximization for all users through the identical IRS phase shift design. For more complex scenarios involving spatial correlation [30], [31], multiple users [29], [30], [32] or non-reciprocity [32], research has typically focused on performance optimization algorithms than the derivation of performance expressions due to mathematical intractability of the latter.

TABLE 1 Comparison With Existing IRS/RIS FD Literature

Paper	Channel	FD	RSI, HI	Devices	Metrics
[24]	Nakagami	FD DF user relay	RSI: constant	an IRS, two users	OP
[25]	Nakagami	One FD DF relay	RSI: Nakagami	one/two RISs, a source, a destination	OP SE BER
[26]	Indoor, outdoor reciprocal	Two-way FD	RSI:$\mathcal{CN}$ HI	a RIS one-pair transceiver	SER OP EC
[27]	Rayleigh reciprocal	Two-way FD	RSI:$\mathcal{CN}$ HI	a RIS two terminals	EC SER
[28]	Rayleigh reciprocal	Two-way FD	RSI:$\mathcal{CN}$	N RISs two terminals	OP EC
[29]	Rician	One-way FD	HI: $\mathcal{CN}$	a RIS K pairs of devices	Optimize achievable rate
[30]	Spatially correlated Rician	Two-way FD	HI: $\mathcal{CN}$	a RIS, K FD user-pairs	Optimize sum-rate
[31]	Correlated Rayleigh	An FD AP	RSI:$\mathcal{CN}$	a STAR-RIS, two HD UEs	Optimize sum-rate
[32]	Rician	Two-way FD	RSI: constant	a RIS, one BS, multiple users	Maximize minimum user rate
Our work	**Rician Nakagami reciprocal non-reciprocal**	Two-way FD	RSI:$\mathcal{CN}$	an IRS, Two FD Users	OP EC

Inspired primarily by the reciprocal and non-reciprocal FD models in [23], in this paper we conduct an analysis on the user performance for an IRS-assisted FD network by taking more realistic Rician and Nakagami fadings into account. It is worthy to highlight that IRS-enabled communications are generally characterized by both, a line-of-sight (LoS) and a non-LoS (NLoS) components, rendering the Rician or Nakagami distribution an appropriate candidate for modeling wireless links in IRS systems. The most available FD papers are devoted to reciprocal channels where Gamma distribution of composite IRS channels are commonly assumed as it is somewhat arduous to analyze non-reciprocal channels. We are concerned whether Gamma distribution can achieve the same accuracy for Rician and Nakagami channels. This issue would provide insight into the methods and results of performance analysis under both channels. The contributions are outlined as below.

- We propose a comprehensive mathematical framework for the performance investigation on an IRS-assisted FD communication system over LoS channels including both Rician and Nakagami fadings, which are regarded as the more realistic assumptions in IRS deployed systems, compared to the Rayleigh fading.

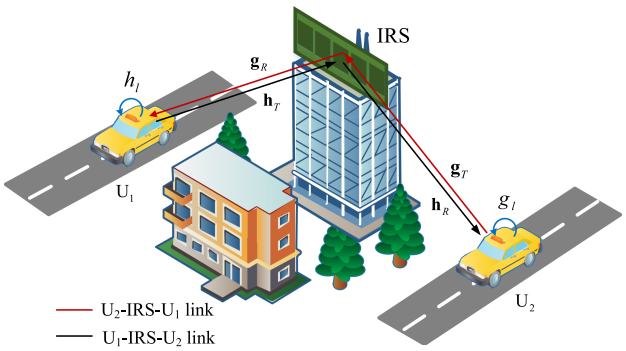

FIGURE 1. An illustration of IRS-assisted full-duplex transmission framework.

- We first derive OP expressions with closed forms in Rician fadings, while considering different distributions for the SINR, namely, non-central Chi-square and Gamma distributions. Then, according to Jensen's inequality, an upper bound of ergodic capacity (EC) is derived. Furthermore, by leveraging the Gauss-Laguerre (GL) and generalized Gauss-Laguerre (GGL) quadrature approximations, we obtain simplified closed forms of the EC based on the CDF and PDF expressions of Gamma distribution.
- We study the exact or approximate OP and EC expressions of FD users with reciprocal and non-reciprocal channels in Nakagami fadings. As regards to the latter, the optimal design of IRS phase shifts allows only one FD user to be prioritized, which renders the performance analysis of the other FD user challenging. We seek an effective solution in this case.
- We provide extensive simulations to demonstrate the exactness of the analytical closed-form expressions, and to provide in-depth insights into the outage and EC performance with regard to the underlying system model under different parameters, including the Rician factor, shape parameter and the associated SI coefficients.

The remainder of this paper is organized as follows. In Section II, the IRS-assisted FD system model is described and the respective SINRs are presented, followed by the derivation of the closed-form expressions of the OP and EC under Rician fading channels in Section III. Sections IV and V present the performance analysis with reciprocal and non-reciprocal channels in Nakagami fadings, respectively. The simulation results are provided in Section VI. Finally, Section VII gives the conclusions.

II. SYSTEM AND CHANNEL MODEL

A. SYSTEM MODEL

Fig. 1 illustrates a FD two-way communication system with a single IRS with N reflective elements, assisting two single-antenna FD users (termed as U_1 and U_2). For a particular scenario, U_1 and U_2 can be viewed as two D2D devices, or a BS and one user. The direct link between the two users is assumed to be obstructed as a result of severe scattering and shadowing, hence, the communication is carried over the IRS link only, using the FD mode. Each FD user consists of two antennas, one for transmitting and the other for receiving, which are located far from each other. Suppose that the channel state information (CSI) over the links related to IRS is perfectly available. In practice, CSI can be acquired by channel estimation technique [23].

The responses of N reflective elements are represented by the diagonal matrix $\Phi = diag\{\phi_1, \ldots, \phi_N\}$, $\phi_i = \beta_i e^{j\theta_i}$, with the amplitude of the ith element denoted by $\beta_i \in [0, 1]$ and its phase shift is denoted by $\theta_i \in [0, 2\pi)$. Following the majority of the literature, we assume a unit amplitude, i.e., $\beta_i = 1$, [33], [34].

In Fig. 1, the channel links from U_1 to U_2 are split into U_1-to-IRS denoted by $\mathbf{h}_T = [h_{T,1}, \ldots, h_{T,N}]^T$ and IRS-to-U_2 represented by $\mathbf{h}_R = [h_{R,1}, \ldots, h_{R,N}]^T$. Similarly, $\mathbf{g}_T = [g_{T,1}, \ldots, g_{T,N}]^T$ and $\mathbf{g}_R = [g_{R,1}, \ldots, g_{R,N}]^T$ denote the channels of U_2-to-IRS link and IRS-to-U_1 link, respectively. It is assumed that all channels are independently identical distributed (i.i.d). In practical application environments, the IRS is generally deployed at the locations where there exist LoS components to both U_1 and U_2, hence all channels may be assumed to obey the Rician or Nakagami distribution.

For the considered FD systems, the channels resulting from the respective transmitting and receiving antennas of U_1 and U_2 are referred to as the SI channels, denoted as h_l and g_l. Thus, the received signals at U_1 and U_2 are denoted, respectively, by

$$y_1 = \underbrace{\sqrt{P_2}\mathbf{g}_R{}^T \Phi \mathbf{g}_T s_2}_{\text{Desired signal}} + \underbrace{\sqrt{P_1}\mathbf{g}_R{}^T \Phi \mathbf{h}_T s_1}_{\text{Reflecting interference}} + \underbrace{\sqrt{P_1} h_l s_1}_{\text{Self interference}} + n_1, \tag{1}$$

$$y_2 = \underbrace{\sqrt{P_1}\mathbf{h}_R{}^T \Phi \mathbf{h}_T s_1}_{\text{Desired signal}} + \underbrace{\sqrt{P_2}\mathbf{h}_R{}^T \Phi \mathbf{g}_T s_2}_{\text{Reflecting interference}} + \underbrace{\sqrt{P_2} g_l s_2}_{\text{Self interference}} + n_2, \tag{2}$$

where $n_i \sim \mathcal{CN}(0, \sigma_i^2)$, $i \in \{1, 2\}$ is the additive white Gaussian noise (AWGN) with the power σ_i^2. Also, s_i denotes the transmit signal at U_i, and P_i is the transmitted power of user U_i, $i \in \{1, 2\}$. Assuming the global CSI is perfectly available at the users, the reflecting interference (RI) can be completely eliminated. Therefore, the received signals at U_1 and U_2 are expressed as

$$y_1 = \sqrt{P_2}\mathbf{g}_R{}^T \Phi \mathbf{g}_T s_2 + w_1 + n_1 \tag{3}$$

$$y_2 = \sqrt{P_1}\mathbf{h}_R{}^T \Phi \mathbf{h}_T s_1 + w_2 + n_2 \tag{4}$$

where w_i, $i \in \{1, 2\}$, is the self-interference signal modelled as $w_i \sim \mathcal{CN}(0, \sigma_{wi}^2)$. Furthermore, the variance of the SI can be modelled as $\sigma_{wi}^2 = t_i P_i^{v_i}$ [23], [35], where the range of two parameters is $t_i > 0$ and $v_i \in [0, 1]$.

Relying on the perfect knowledge of CSI, the phase shifts of the IRS elements are selected to maximize the received signal energy. It is known that maximum signal-to-interference-plus-noise ratio (SINR) will be achieved when the phase shift is

reconfigured as $\theta_n = -\arg(g_{R,n}) - \arg(g_{T,n})$. Thanks to the channel reciprocity, which means that $\mathbf{h_T}$ equals $\mathbf{g_R}$, and $\mathbf{g_T}$ is the same as $\mathbf{h}_R$, the maximum instantaneous SINRs at U_1 and U_2 are evaluated as

$$\gamma_1 = \frac{P_2\left(\sum_{n=1}^{N} |g_{R,n}|\,|g_{T,n}|\right)^2}{\sigma_1^2 + \sigma_{w1}^2} \tag{5}$$

and

$$\gamma_2 = \frac{P_1\left(\sum_{n=1}^{N} |h_{R,n}|\,|h_{T,n}|\right)^2}{\sigma_2^2 + \sigma_{w2}^2}, \tag{6}$$

respectively.

It is highlighted that in the context of channel non-reciprocity, the representation of γ_2 is thought to be unlike (6), as detailed in Section V.

B. CHANNEL MODEL

Take two types of channel models incorporating LoS into account. First, we consier all channels are generated by the Rician distribution, and define the Rician factor as $K_i = A^2/(2\delta^2), i = 1, 2$, K_1 and K_2 corresponding to U_1 and U_2, respectively. And the scale parameter is defined as $B = A^2 + 2\delta^2$, where A^2 and $2\delta^2$ denote the power corresponding to LoS and NLoS components. Assuming a normalized average received power, $B = 1$. Recall that a Rician variable can be formulated by the following probability density function (PDF)

$$f_Z(z) = \frac{z}{\delta^2}\exp\left(-\frac{z^2 + A^2}{2\delta^2}\right) I_0\left(\frac{zA}{\delta^2}\right), z > 0, \tag{7}$$

where $I_v(\cdot)$ denotes a v-order modified Bessel function of the first kind.

Secondly, assume all channels obey the Nakagami distribution, and the PDF expression for the Nakagami channel envelopes X_i is given by

$$f_{X_i}(x) = \frac{2{m_i}^{m_i}}{\Gamma(m_i)\,{\Omega_i}^{m_i}} x^{2m_i - 1}\exp\left(-\frac{m_i}{\Omega_i}x^2\right). \tag{8}$$

III. PERFORMANCE ANALYSIS IN RICIAN FADINGS

In this section, the thorough performance study is conducted for considered system where all channels undergo Rician fadings. The closed-form expressions for outage probability are presented under the non-central Chi-square and Gamma distribution assumptions on the users' SINR. Then, we provide an upper bound and two closed-form solutions for ergodic capacity.

A. OUTAGE PROBABILITY

From (5) and (6), the system will be in an outage when at least one user experiences an outage, that is, when γ_1 or γ_2 falls below its specified SINR threshold [22], i.e. γ_{th_1} or γ_{th_2}, respectively. Therefore, the overall outage probability of the considered system can be represented by

$$\begin{aligned} \text{P}_{\text{out}} &= \Pr\left\{\left\{\gamma_1 < \gamma_{\text{th}_1}\right\} \cup \left\{\gamma_2 < \gamma_{\text{th}_2}\right\}\right\} \\ &= \text{P}_{\text{out1}} + P_{\text{out2}} - P_{\text{out1}}P_{\text{out2}} \end{aligned} \tag{9}$$

where the outage probabilities of U_1 and U_2 are given by

$$\text{P}_{\text{out1}} = \Pr\left(\gamma_1 < \gamma_{\text{th}_1}\right) \tag{10}$$

$$\text{P}_{\text{out2}} = \Pr\left(\gamma_2 < \gamma_{\text{th}_2}\right) \tag{11}$$

In what follows, we perform the analyses on the outage probability and ergodic capacity at U_1. Similar approach can apply to U_2.

1) NON-CENTRAL CHI-SQUARE DISTRIBUTION ASSUMPTION ON SINR

The derivation of outage probability is dependent on the statistical distribution of the users' SINR, which can be assumed to be non-central Chi-square distribution resulted from the central limit theorem (CLT) in this subsection.

Theorem 1: Under the non-central Chi-square distribution assumption on the SINR, the closed-form outage probability for U_1 can be given by

$$P_{\text{out1}} = 1 - \text{Q}_{\frac{1}{2}}\left(\sqrt{\lambda}, \sqrt{\frac{\gamma_{\text{th}_1}}{\sigma^2\rho}}\right) \tag{12}$$

where $\text{Q}_M(a, b)$ is the generalized Marcum Q function, and

$$\rho = \frac{P_2}{{\sigma_1}^2 + \sigma_{w1}^2}, \tag{13}$$

$$\lambda = \frac{N}{\frac{16(K_1+1)(K_2+1)}{\pi^2\left(\text{L}_{\frac{1}{2}}(-K_1)\right)^2\left(\text{L}_{\frac{1}{2}}(-K_2)\right)^2} - 1} \tag{14}$$

and

$$\sigma^2 = N - \frac{N\pi^2}{16\,(K_1+1)\,(K_2+1)}\left(\text{L}_{\frac{1}{2}}(-K_1)\right)^2\left(\text{L}_{\frac{1}{2}}(-K_2)\right)^2, \tag{15}$$

where the Laguerre polynomial $\text{L}_{1/2}(x) = e^{x/2}[(1 - x)I_0(\frac{-x}{2}) - xI_1(\frac{-x}{2})]$.

Proof: From (5) and (10), we evaluate the outage probability at U_1 as

$$P_{\text{out1}} = \Pr\left(u^2 < \frac{\gamma_{\text{th}_1}}{\rho}\right), \tag{16}$$

where $u = \sum_{n=1}^{N} |g_{R,n}||g_{T,n}|$. Due to the mutual independence between $|g_{T,n}|$ and $|g_{R,n}|$ and given that both of them follow the Rician distribution in (7), their statistical characteristics are given by

$$\mathbb{E}\left\{|g_{R,n}|\right\} = \sqrt{\frac{\pi}{4\,(K_1+1)}}\text{L}_{\frac{1}{2}}(-K_1), \tag{17}$$

$$\mathbb{E}\left\{|g_{T,n}|\right\} = \sqrt{\frac{\pi}{4\,(K_2+1)}}\text{L}_{\frac{1}{2}}(-K_2), \tag{18}$$

$$\begin{aligned} \mathbb{E}\left\{|g_{R,n}|\,|g_{T,n}|\right\} &= \frac{\pi}{4\sqrt{(K_1+1)\,(K_2+1)}} \\ &\quad \times \text{L}_{\frac{1}{2}}(-K_1)\,\text{L}_{\frac{1}{2}}(-K_2), \end{aligned} \tag{19}$$

$$\mathbb{E}\left\{\left|g_{R,n}\right|^2\right\} = A^2 + 2\delta^2 = 1, \quad \mathbb{E}\left\{\left|g_{T,n}\right|^2\right\} = 1, \tag{20}$$

$$\mathbb{E}\left\{\left|g_{R,n}\right|^2\left|g_{T,n}\right|^2\right\} = 1, \tag{21}$$

and

$$\begin{aligned}&\mathrm{Var}\left\{\left|g_{R,n}\right|\left|g_{T,n}\right|\right\}\\ &= 1 - \frac{\pi^2}{16\left(K_1+1\right)\left(K_2+1\right)}\left(\mathrm{L}_{\frac{1}{2}}\left(-K_1\right)\right)^2\left(\mathrm{L}_{\frac{1}{2}}\left(-K_2\right)\right)^2.\end{aligned} \tag{22}$$

Utilizing the CLT, for a sufficiently large N, we model u as being normally distributed $u \sim \mathcal{N}(\mu, \sigma^2)$, where $\mu = \sum_{n=1}^{N} \mathbb{E}\{|g_{R,n}||g_{T,n}|\}$ and $\sigma^2 = \sum_{n=1}^{N} \mathrm{Var}\{|g_{R,n}||g_{T,n}|\}$. From (19) and (22), μ and σ^2 are calculated as

$$\mu = \frac{N\pi}{4\sqrt{\left(K_1+1\right)\left(K_2+1\right)}}\mathrm{L}_{\frac{1}{2}}\left(-K_1\right)\mathrm{L}_{\frac{1}{2}}\left(-K_2\right) \tag{23}$$

and

$$\sigma^2 = N - \frac{N\pi^2}{16\left(K_1+1\right)\left(K_2+1\right)}\left(\mathrm{L}_{\frac{1}{2}}\left(-K_1\right)\right)^2\left(\mathrm{L}_{\frac{1}{2}}\left(-K_2\right)\right)^2. \tag{24}$$

Since u/σ is a random variable with normally distributed similar to u, it has the mean μ/σ and unit variance. It follows that $(u/\sigma)^2$ can be modeled as a non-central chi-square (NCC) random variable, namely $(u/\sigma)^2 \sim \chi^2(\kappa, \lambda)$, wherein $\kappa = 1$ denotes the degree of freedom, and $\lambda = \mu^2/\sigma^2$ is the non-centrality parameter with yielding

$$\lambda = \frac{N\pi^2\left(\mathrm{L}_{\frac{1}{2}}\left(-K_1\right)\right)^2\left(\mathrm{L}_{\frac{1}{2}}\left(-K_2\right)\right)^2}{16\left(K_1+1\right)\left(K_2+1\right) - \pi^2\left(\mathrm{L}_{\frac{1}{2}}\left(-K_1\right)\right)^2\left(\mathrm{L}_{\frac{1}{2}}\left(-K_2\right)\right)^2}. \tag{25}$$

Apparently, (25) can be reduced to (14).

By exploiting the cumulative distribution function (CDF) of the NCC variable, the outage probability of U_1 in (16) can be rewritten as

$$\begin{aligned}P_{\mathrm{out1}} &= \Pr\left(\rho u^2 < \gamma_{\mathrm{th}_1}\right)\\ &= \Pr\left(\left(\frac{u}{\sigma}\right)^2 < \frac{\gamma_{\mathrm{th}_1}}{\sigma^2\rho}\right)\\ &= 1 - \mathrm{Q}_{\frac{1}{2}}\left(\sqrt{\lambda}, \sqrt{\frac{\gamma_{\mathrm{th}_1}}{\sigma^2\rho}}\right).\end{aligned} \tag{26}$$

For the ease of computer simulation, the Marcum Q function is able to be replaced by its equivalent form [36]

$$\mathrm{Q}_{\frac{1}{2}}(a, b) = \frac{1}{2}\left[\mathrm{erfc}\left(\frac{b-a}{\sqrt{2}}\right) + \mathrm{erfc}\left(\frac{b+a}{\sqrt{2}}\right)\right] \tag{27}$$

■

On account of channel reciprocity, the analytical outage probability at U_2 is deduced as

$$P_{\mathrm{out2}} = 1 - \mathrm{Q}_{\frac{1}{2}}\left(\sqrt{\lambda}, \sqrt{\frac{\gamma_{\mathrm{th}_2}}{\sigma^2 P_1}\left(\sigma_2{}^2 + \sigma_{w2}{}^2\right)}\right) \tag{28}$$

2) GAMMA DISTRIBUTION ASSUMPTION ON SINR

In our earlier paper [37], u is modeled as the gamma distribution in the context of Rayleigh fading channels. For the considered Rician fading scenarios, we can also regard u as the gamma distribution, and thus deduce the PDF and CDF expressions of the SINR as Theorem 2.

Theorem 2: Under the Gamma distribution assumption on SINR, the PDF and CDF of γ_1 are given by

$$f_{\gamma_1}(z) = \frac{z^{\frac{\Lambda-1}{2}}}{2\Omega^{\Lambda+1}\Gamma\left(\Lambda+1\right)\rho^{\frac{\Lambda+1}{2}}}\exp\left(-\frac{\sqrt{z}}{\Omega\sqrt{\rho}}\right), \tag{29}$$

and

$$F_{\gamma_1}(z) = \frac{\gamma\left(\Lambda+1, \frac{\sqrt{z}}{\Omega\sqrt{\rho}}\right)}{\Gamma\left(\Lambda+1\right)}, \tag{30}$$

where

$$\Lambda = \frac{\mathbb{E}^2(u)}{\mathrm{Var}(u)} - 1 = \frac{\mu^2}{\sigma^2} - 1, \tag{31}$$

and

$$\Omega = \frac{\mathrm{Var}(u)}{\mathbb{E}(u)} = \frac{\sigma^2}{\mu}. \tag{32}$$

Specifically, the mean and variance of u are given by (23) and (24), respectively, $\gamma(\cdot)$ denotes the lower incomplete gamma function and $\Gamma(\cdot)$ is the complete gamma function.

Based on (10) and (30), the closed-form outage probability at U_1 is given by

$$P_{\mathrm{out1}} = \Pr\left(\gamma_1 < \gamma_{\mathrm{th}_1}\right) = \mathrm{F}_{\gamma_1}\left(\gamma_{\mathrm{th}_1}\right) = \frac{\gamma\left(\Lambda+1, \frac{\sqrt{\gamma_{\mathrm{th}_1}}}{\Omega\sqrt{\rho}}\right)}{\Gamma\left(\Lambda+1\right)}. \tag{33}$$

B. ERGODIC CAPACITY

In this subsection, apart from an upper bound, the rigorous approximations of evaluating the ergodic capacity will be explored.

The ergodic capacity of U_1 is computed by

$$C = \mathbb{E}\left\{\log_2(1+\gamma_1)\right\} \tag{34}$$

1) AN UPPER BOUND

By leveraging the Jensen's inequality, Theorem 3 provides an analytical expression for the upper bound on the ergodic capacity.

Theorem 3: An upper bound on the ergodic capacity of U_1 is given as in closed form

$$\begin{aligned}C_{up} = \log_2\Bigg(&1 + \rho N + \rho M\\ &\times\left(\mathrm{L}_{\frac{1}{2}}\left(-K_1\right)\right)^2\left(\mathrm{L}_{\frac{1}{2}}\left(-K_2\right)\right)^2\Bigg),\end{aligned} \tag{35}$$

where $M = \frac{N(N-1)\pi^2}{16(K_1+1)(K_2+1)}$.

Proof: It follows from Jensen's inequality that the upper bound of the ergodic capacity is

$$C \leq \log_2\left(1 + \mathbb{E}\left\{\gamma_1\right\}\right) = C_{up}. \tag{36}$$

Leveraging the binomial expansion theorem to expand γ_1 yields

$$\begin{aligned}\mathbb{E}\{\gamma_1\} &= \rho\mathbb{E}\left\{\left(\sum_{i=1}^{N}\left|g_{R,i}\right|\left|g_{T,i}\right|\right)^2\right\} \\ &= \rho\left(\mathbb{E}\left\{\sum_{i=1}^{N}\left|g_{R,i}\right|^2\left|g_{T,i}\right|^2\right\}\right. \\ &\quad \left.+\mathbb{E}\left\{\sum_{i=1}^{N}\sum_{\substack{j=1\\ j\neq i}}^{N}\left|g_{R,i}\right|\left|g_{T,i}\right|\left|g_{R,j}\right|\left|g_{T,j}\right|\right\}\right).\end{aligned} \tag{37}$$

Relying on the independence assumption between the Rician channels, and from (21), we have

$$\mathbb{E}\left\{\sum_{j=1}^{N}\left|g_{R,j}\right|^2\left|g_{T,j}\right|^2\right\} = N. \tag{38}$$

Additionally, it follows from (17) and (18) that

$$\begin{aligned}&\mathbb{E}\left\{\sum_{n=1}^{N}\sum_{\substack{j=1\\ j\neq n}}^{N}\left|g_{R,n}\right|\left|g_{T,n}\right|\left|g_{R,j}\right|\left|g_{T,j}\right|\right\} \\ &= \frac{N(N-1)\pi^2}{16\left(K_1+1\right)\left(K_2+1\right)}\left(\mathrm{L}_{\frac{1}{2}}\left(-K_1\right)\right)^2\left(\mathrm{L}_{\frac{1}{2}}\left(-K_2\right)\right)^2.\end{aligned} \tag{39}$$

Hence, from (38) and (39), we obtain

$$\begin{aligned}\mathbb{E}\left\{\gamma_1\right\} = \rho\left(N + \frac{N(N-1)\pi^2}{16\left(K_1+1\right)\left(K_2+1\right)}\right. \\ \left.\times\left(\mathrm{L}_{\frac{1}{2}}\left(-K_1\right)\right)^2\left(\mathrm{L}_{\frac{1}{2}}\left(-K_2\right)\right)^2\right).\end{aligned} \tag{40}$$

By inserting (40) into (36), the upper bound in (35) can be obtained. ■

Remark 1: Since $\mathrm{L}_{1/2}(-K)$ is a monotonically increasing function of K, The ergodic capacity ascends as K becomes larger. Moreover, the ergodic capacity is primarily determined by $\log_2(N(N-1))$, which indicates that the increasing N can raise ergodic capacity considerably.

2) APPROXIMATED ERGODIC CAPACITY

Based on Theorem 2, the ergodic capacity of U_1 is calculated as

$$\begin{aligned}C &= \mathbb{E}\left\{\log_2(1+\gamma_1)\right\} \\ &= \int_0^{+\infty}\log_2(1+z)f_{\gamma_1}(z)dz \\ &= \frac{1}{\ln 2}\int_0^{+\infty}\frac{1-F_{\gamma_1}(z)}{1+z}dz,\end{aligned} \tag{41}$$

where $f_{\gamma_1}(z)$ and $F_{\gamma_1}(z)$ are given by (29) and (30), respectively.

Due to the mathematical intractability of (41), we exploit the Gauss quadrature methods, including the Gauss-Laguerre (GL) quadrature, generalized Gauss-Laguerre (GGL) quadrature [38], [39].

In this subsection, we adopt the above-mentioned approaches in order to obtain a satisfactory approximation for the ergodic capacity.

Method 1: Gauss-Laguerre Quadrature

We first select GL quadrature to reap the solution of (41), as given in Theorem 4.

Theorem 4: By employing the Gauss-Laguerre quadrature approximation, the ergodic capacity of U_1 can be formulated as

$$C \approx \frac{1}{\ln 2}\sum_{\ell=1}^{G}\omega_\ell e^{x_\ell}\frac{1-F_{\gamma_1}(x_\ell)}{1+x_\ell}. \tag{42}$$

Proof: Recall that the Gauss-Laguerre quadrature method is represented as

$$\int_0^{\infty} f(x)dx \approx \sum_{\ell=1}^{G}\omega_\ell e^{x_\ell} f\left(x_\ell\right), \tag{43}$$

where G is the order of a Laguerre polynomial $L_G(x)$, and x_ℓ is the ℓth root of $L_G(x)$, whose series representation is written as

$$L_G(x) = \sum_{i=0}^{G}(-1)^i\frac{G!}{(i!)^2(G-i)!}x^i, \tag{44}$$

and the ℓth weight is

$$w_\ell = \frac{x_\ell}{(G+1)^2\left(L_{G+1}\left(x_\ell\right)\right)^2}. \tag{45}$$

Using (43), the integral in (41) can be accurately evaluated as

$$C \approx \frac{1}{\ln 2}\sum_{\ell=1}^{G}\omega_\ell e^{x_\ell}\frac{1-F_{\gamma_1}(x_\ell)}{1+x_\ell}. \tag{46}$$

■

Method 2: Generalized Gauss-Laguerre Quadrature

Considering the drawbacks that Gauss-Laguerre quadrature requires a higher order G to achieve a satisfactory approximation, as an alternative, the generalized Gauss-Laguerre quadrature is taken into account. We reformulate the ergodic capacity as

$$\begin{aligned}C &= \int_0^{+\infty}\log_2(1+z)f_{\gamma_1}(z)dz \\ &= \frac{1}{\ln 2}\int_0^{+\infty}\frac{z^{\frac{\Lambda-1}{2}}\ln(1+z)}{2\Omega^{\Lambda+1}\Gamma(\Lambda+1)\rho^{\frac{\Lambda+1}{2}}}\exp\left(-\frac{\sqrt{z}}{\Omega\sqrt{\rho}}\right)dz\end{aligned}$$

$$= \frac{1}{\ln 2}\int_0^{+\infty} \frac{\ln\left(1+t^2\right)}{\Omega^{\Lambda+1}\Gamma(\Lambda+1)\rho^{\frac{\Lambda+1}{2}}} t^{\Lambda}\exp\left(-\frac{t}{\Omega\sqrt{\rho}}\right)dt$$

$$= \frac{1}{\Gamma(\Lambda+1)\ln 2}\int_0^{+\infty} x^{\Lambda}e^{-x}\ln\left(1+\Omega^2\rho x^2\right)dx. \quad (47)$$

The GGL quadrature can be utilized to solve (47), as given in Theorem 5.

Theorem 5: Based on the GGL quadrature, the closed form of the ergodic capacity of U_1 is formulated as

$$C \approx \frac{1}{G!(G+1)^2\ln 2}\sum_{i=1}^{G}\frac{(\Lambda+1)_G x_i \ln\left(1+\Omega^2\rho x_i^2\right)}{\left(L_{G+1}^{\Lambda}(x_i)\right)^2}. \quad (48)$$

Proof: Recall that the generalized Gauss-Laguerre quadrature rule is expressed as [40]

$$\int_0^{\infty} x^a e^{-x} g(x)dx \approx \sum_{k=1}^{G}\omega_k \cdot g(x_k) \quad (49)$$

where w_i denotes the ith weight,

$$w_i = \frac{\Gamma(G+a+1)x_i}{G!(G+1)^2\left(L_{G+1}^{a}(x_i)\right)^2}, \quad (50)$$

and x_i is the ith root of the generalized Laguerre polynomial of $L_G^a(x)$, with the order G.

From (47) and (49), we can obtain

$$C \approx \frac{1}{\Gamma(\Lambda+1)\ln 2}\sum_{i=1}^{G} w_i \ln\left(1+\Omega^2\rho x_i^2\right). \quad (51)$$

It is worth mentioning that $\Gamma(\Lambda+1)$ approaches infinity when Λ is large, due to the limited precision of common mathematical platforms, such as Matlab, and hence, an accurate evaluation of C using (51) is not easy to obtain. As a consequence, by substituting (50) into (51), whose equivalent form is converted into (48), where $(a)_n = \frac{\Gamma(a+n)}{\Gamma(a)}$ is a Pochhammer symbol. ■

Remark 2: Through the numerical simulation in Section IV, it is shown that the analytical values in (42) and (48) can match well with the Monte Carlo result. However, the generalized Laguerre quadrature still performs well for small order G, even $G = 1$, whereas the method 1 needs greater G. This implies that method 2 enjoys powerful fitting capability in the quadrature scenarios involving infinite integral limits. Meanwhile, to some extent, the less number of weight and root coefficients reduces the storage and computational burden as far as performance analysis is concerned.

IV. PERFORMANCE ANALYSIS IN NAKAGAMI FADINGS

In order to further evaluate the validity of Gamma distribution assumption on SINR, instead of Rician fading, the performance analysis is investigated over the Nakagami fading channels in this section.

A. OUTAGE PROBABILITY

Theorem 6: For Nakagami fading channels, the closed-form outage probability for user U_1 is

$$P_{\text{out1}} = \frac{\gamma\left(\tilde{\Lambda}+1, \frac{\sqrt{\gamma_{th1}}}{\tilde{\Omega}\sqrt{\rho}}\right)}{\Gamma\left(\tilde{\Lambda}+1\right)}, \quad (52)$$

where

$$\tilde{\Lambda} = \frac{\tilde{\mu}^2}{\tilde{\sigma}^2} - 1, \quad (53)$$

and

$$\tilde{\Omega} = \frac{\tilde{\sigma}^2}{\tilde{\mu}}, \quad (54)$$

with

$$\tilde{\mu} = N\frac{\Gamma\left(m_1+\frac{1}{2}\right)\Gamma\left(m_2+\frac{1}{2}\right)}{\Gamma(m_1)\Gamma(m_2)}\left(\frac{\Omega_1\Omega_2}{m_1 m_2}\right)^{\frac{1}{2}}, \quad (55)$$

and

$$\tilde{\sigma}^2 = N\Omega_1\Omega_2\left(1-\frac{1}{m_1 m_2}\frac{\Gamma\left(m_1+\frac{1}{2}\right)^2\Gamma\left(m_2+\frac{1}{2}\right)^2}{\Gamma(m_1)^2\Gamma(m_2)^2}\right). \quad (56)$$

Proof: The mean of the Nakagami channels from U_2 to U_1 can be obtained as

$$\mathbb{E}\left\{|g_{R,n}|\right\} = \frac{\Gamma\left(m_1+\frac{1}{2}\right)}{\Gamma(m_1)}\left(\frac{\Omega_1}{m_1}\right)^{\frac{1}{2}}. \quad (57)$$

$$\mathbb{E}\left\{|g_{T,n}|\right\} = \frac{\Gamma\left(m_2+\frac{1}{2}\right)}{\Gamma(m_2)}\left(\frac{\Omega_2}{m_2}\right)^{\frac{1}{2}}. \quad (58)$$

Due to the independence between the channels, it follows that,

$$\mathbb{E}\left\{|g_{T,n}||g_{T,n}|\right\} = \frac{\Gamma\left(m_1+\frac{1}{2}\right)\Gamma\left(m_2+\frac{1}{2}\right)}{\Gamma(m_1)\Gamma(m_2)}\left(\frac{\Omega_1\Omega_2}{m_1 m_2}\right)^{\frac{1}{2}}, \quad (59)$$

$$\mathbb{E}\left\{|g_{R,n}|^2|g_{T,n}|^2\right\} = \mathbb{E}\left\{|g_{R,n}|^2\right\}\mathbb{E}\left\{|g_{T,n}|^2\right\} = \Omega_1\Omega_2, \quad (60)$$

$$\text{Var}\left\{|g_{R,n}||g_{T,n}|\right\} = \Omega_1\Omega_2\left(1-\frac{1}{m_1 m_2}\frac{\Gamma\left(m_1+\frac{1}{2}\right)^2\Gamma\left(m_2+\frac{1}{2}\right)^2}{\Gamma(m_1)^2\Gamma(m_2)^2}\right). \quad (61)$$

Consequently, the mean and variance of $u = \sum_{n=1}^{N}|g_{R,n}||g_{T,n}|$ are given as (55) and (56), respectively.

The analytical outage probability of U_1 resembles to (33), as manifested in Theorem 6. ■

Remark 3: When the channels experience Rician fading, the analytical outage probability curves with log scaling along Y-axis gradually exhibit slight deviation from the Monte Carlo results as the SNR increases whereas the ones with linear scaling along Y-axis can fit well over the whole SNR range. On the

other hand, when the channels experience Nakagami fading, the analytical outage probability curves with log and linear scalings along Y-axis can match well with the Monte Carlo ones over the entire SNR region. These phenomena reveal that the Gamma distribution assumption on SINR over Nakagami fading can achieve more precise approximation than that over Rician fading.

B. ERGODIC CAPACITY

On account of the identical gamma distribution assumptions on the SINR for Rician and Nakagami fadings, the approximate expressions with respect to ergodic capacity in Theorems 4 and 5 are still apllicable to this situation. Nevertheless, it is notable that the Λ and Ω involving into (42) and (48) should be replaced with (55) and (56) accordingly.

Remark 4: As observed in the ensuing simulation figures, the tight approximations can be achieved in both Rician and Nakagami fadings. Apart from the correct derivation, this is possibly due to the accuracy limitation of linear vertical coordinates that does not allow for finer distinctions.

V. PERFORMANCE ANALYSIS WITH NON-RECIPROCAL CHANNELS IN NAKAGAMI FADINGS

The above analysis considers the situation where the channels of two users are reciprocal for FD systems. In this section, we examine the case with non-reciprocal channels. In this scenario, once the optimal phase configuration of IRS is fixed for one user (assmuing U_1), the other user (U_2) is supposed to have imperfect phase configuration thanks to the channel disparity with U_1. There exists the non-negligible phase error for U_2. At this regard, the SINR of U_2 is given by

$$\gamma_2 = \frac{P_1}{{\sigma_2}^2 + {\sigma_{w2}}^2}\left|\sum_{n=1}^{N} h_{R,n}h_{T,n}e^{j\theta_n}\right|^2 \tag{62}$$

Recall that in (62), θ_n has been determined according to the channel phases of U_1, namely $\theta_n = -\arg(g_{R,n}) - \arg(g_{T,n})$. The preceding analysis process is no longer applicable to U_2.

A. OUTAGE PROBABILITY OF U_2

In the context of Nakagami fading, the outage probability $\mathrm{P}_{\mathrm{out2}} = \Pr(\gamma_2 < \gamma_{\mathrm{th}_2})$ of U_2 can be evaluted as Theorem 7. The detailed derivation process refers to [41].

Theorem 7: For Nakagami fading channels, the closed-form outage probability for user U_2 is expressed as

$$P_{\mathrm{out2}} = \sum_{c_1=0}^{m_1-1}\cdots\sum_{c_N=0}^{m_1-1}\prod_{i=1}^{N}\frac{(m_2)_{m_1-1-c_i}\,(1-m_2)_{c_i}}{(m_1-1-c_i)!c_i!} \times\left(1-\frac{2}{(d-1)!}\left(\sqrt{\frac{m_1m_2\gamma_{th2}}{\Omega_1\Omega_2\rho_2}}\right)^d K_d\left(2\sqrt{\frac{m_1m_2\gamma_{th2}}{\Omega_1\Omega_2\rho_2}}\right)\right), \tag{63}$$

where $\rho_2 = \frac{P_1}{{\sigma_2}^2+\sigma_{w2}^2}$, $d = N(m_1+m_2-1) - \sum_{i=1}^{N} c_i$, $(m)_c$ is the Pochhammer symbol, and $K_d(\cdot)$ denotes the modified Bessel function of the second kind with the dth order.

B. ERGODIC CAPACITY OF U_2

The exact expressions of $C_2 = \mathbb{E}\{\log_2(1+\gamma_2)\}$ can be expressed as in a closed-form [41]

$$C_2 = \frac{1}{\ln 2}\sum_{c_1=0}^{m_1-1}\cdots\sum_{c_N=0}^{m_1-1}\prod_{i=1}^{N}\frac{(m_2)_{m_1-1-c_i}\,(1-m_2)_{c_i}}{(m_1-1-c_i)!c_i!} \times\frac{1}{(d-1)!}G_{3,1}^{1,3}\left(\frac{\rho_2\Omega_1\Omega_2}{m_1m_2}\,\middle|\,\begin{matrix}1,1,1-d\\1\end{matrix}\right). \tag{64}$$

Remark 5: The results from (63) and (64) can coincide with corresponding Monte Carlo simulation ones, provided by Section VI.C. When $m_1 = 1$ or $m_2 = 1$, which means that the corresponding channel reduces to Rayleigh fading, the above derivations still hold.

VI. NUMERICAL RESULTS

In this section, the concerned performance is numerically evaluated for the considered IRS-assisted FD system. In the following simulations, the adopted parameters are given by as below. The transmit power and noise power of U_1 and U_2 are set as $P_1 = P_2 = P$, $\sigma_1^2 = \sigma_2^2 = 1$, respectively. The SINR threshold is set to $\gamma_{\mathrm{th}_1} = \gamma_{\mathrm{th}_2} = -10$˜dB, and the Rician factor $K_1 = K_2 = K$. Using Monte Carlo simulations (marked as 'sim' in the legends) as the benchmark, we substantiate the correctness of the preceding theoretical results, marked as 'ana' in the legends.

A. PERFORMANCE WITH RECIPROCAL CHANNELS

1) OUTAGE PERFORMANCE

Fig. 2 depicts the closed-form outage probabilities for U_1 under two distribution approximations with different numbers of IRS elements $N = 8, 16, 32$ and Rician factors $K = 3, 5$, where the self-interference variance for user U_1 is $\sigma_{w1}^2 = 3$ dB and the SI parameters are set to be $t_1 = 3$ dB and $v_1 = 0$. Fig. 2(a) shows the derived outage probability in (12) based on the non-central chi-squared distribution approximation, and Fig. 2(b) displays the derived outage probability in (33) based on the Gamma distribution approximation. Apparently, the outage probability degrades sharply with the increment of transmit power, meanwhile decreases rapidly with the increase of N. In addition, the decay rate of the outage probability increases with an increase in the Rician factor K. We can observe that the outage probabilities based on Gamma distribution assumptions are completely consistent with Monte Carlo simulations in all cases. Moreover, for the small number of IRS elements, the analytical results associated with the non-central chi-square distribution deviate from the actual ones.

Fig. 3 presents the outage performance of U_1 in the context of Nakagami fading for SINR threshold γ_{th1}=0 dB, which also reflects the effect of the numbers of IRS elements given $m = 3$ and $\Omega = 1$. From this figure, we can observe that both the analysis results and Monte Carlo ones overlap exactly within the whole SNR region, which implies that the gamma approximation of SINR is remarkably satisfactory in Nakagami channels.

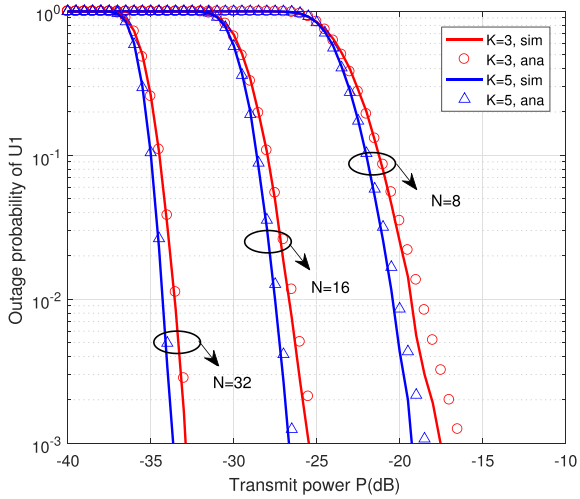

FIGURE 2. Outage probability of user U_1 with different IRS reflection elements in Rician fading channels. (a) Outage probability based on non-central chi-square distribution approximation; (b) Outage probability based on Gamma distribution approximation.

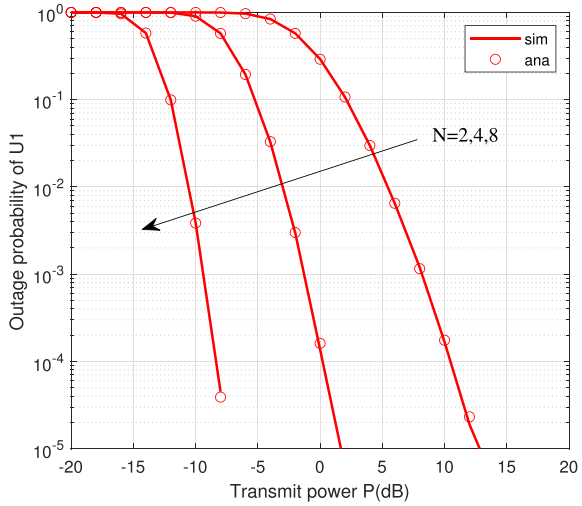

FIGURE 3. Impact of the number of IRS elements on U_1 outage performance in Nakagami-m fading channels.

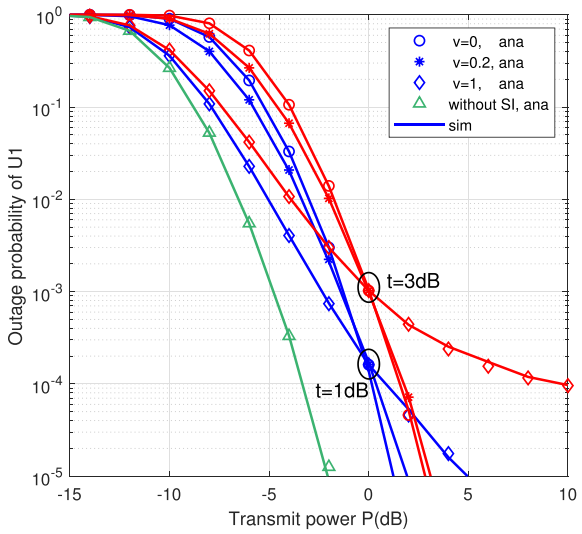

FIGURE 4. Influence of SI coefficients on U_1's outage probability under Nakagami fading, $m = 3$, $\Omega = 1$, $N = 4$.

In Fig. 4, we plot the impact of varied SI coefficients on the outage probability of user U_1, under Nakagami-m fading where $m = 3$, $\Omega = 1$, $N = 4$, $\gamma_{th1} = 0\,dB$. It is seen that the analytical result in Theorem 6 exactly coincides with the Monte Carlo simulation counterpart. As deduced from $\sigma_{wi}^2 = t_i P_i^{v_i}$, the less SI variance with smaller t results in the lower outage probability. Meanwhile, for fixed t, the less variance with increasing v degrades the outage probability when the transmit power is less than 0 dB; when the transmit power is greater than 0 dB, the opposite is the case; when P=0 dB, the identical outage performance is observed. In addition, there exists the obvious performance gap with the increase of SNR compared to the case without SI.

2) ERGODIC CAPACITY

In Fig. 5, we depict the performance of the derived upper bound on the ergodic capacity, the analytical results based on Theorems 4 and 5, along with the Monte Carlo simulation for different numbers of IRS elements. It can be observed that the analytical results based on GL quadrature and GGL quadrature coincide with Monte Carlo values for arbitrary number of IRS elements. For the GGL quadrature, the less order can achieve higher accuracy. Furthermore, there is a mismatch between the upper bound in Theorem 3 and the simulated value for $N = 1$. As expected, this upper bound becomes tight when N is large.

Fig. 6 characterizes the influence of the number of IRS elements on the ergodic capacity at different transmit powers, where the GGL quadrature is adopted (G=1). It can be

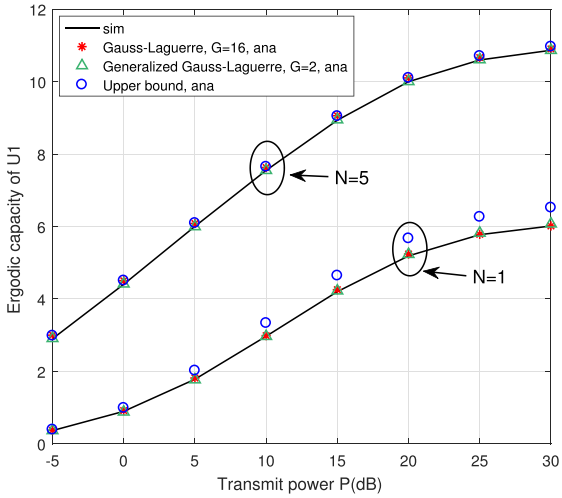

FIGURE 5. Ergodic capacity of U_1.

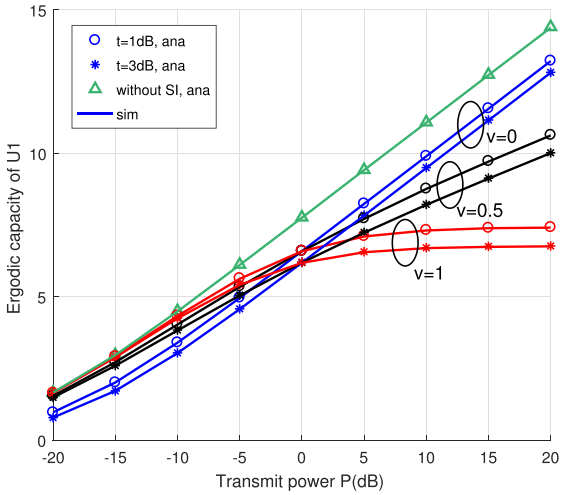

FIGURE 7. Impact of SI coefficients on U_1's ergodic capacity, $K = 5$, $N = 16$.

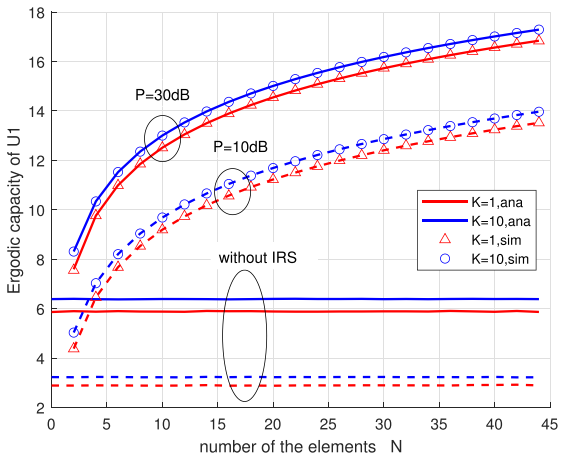

FIGURE 6. Ergodic capacity of U_1 vs. the number of IRS elements.

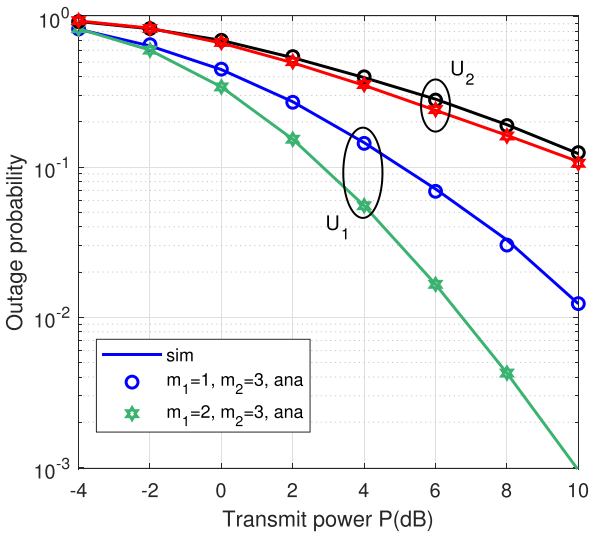

FIGURE 8. Outage performance of U_1 and U_2, $N = 2$.

noticed that IRS technology greatly contribute to the capacity enhancement in contrast with no IRS. As expected, the system performance can be improved by the increment of some parameters such as the number of IRS elements, transmit power as well as Rician factor.

In Fig. 7, we present the effect of the SI coefficients on U_1's ergodic capacity, for $K = 5$, $N = 16$, with perfect and imperfect SI. We can observe the exactly overlapped curves between the closed forms and the simulation ones. Additionally, for the same v, as t increases, the ergodic capacity degrades. The ergodic capacity increases with increasing v when transmit power $P < 0$ is less than 0 dB while the ergodic capacity performs the opposite with increasing v when the transmit power P is greater than 0 dB. This is because v determines the amount of self-interference σ_{w1}^2 associated with transmit power.

It is worth clarifying that Figs. 5–7 are simulated in Rician fading channels since the obtained curves in the case of Nakagami fading perform the similar results.

B. PERFORMANCE WITH NON-RECIPROCAL CHANNELS

Considering the Nakagami fadings, we focus on evaluating the outage performance and ergodic capacity for U_2 with non-reciprocal channels. In Figs. 8 and 9, where $N = 2$, $\Omega_1 = \Omega_2 = 1$ and $\gamma_{th1} = \gamma_{th2} = 1$, we readily observe the consistency between the analytical values in (63) and the simulations. Fig. 8 manifests the inferior performance of U_2 with the nonideal IRS phase configuration in contrast to U_1 with the optimal phase. It also shows the larger performance difference between U_1 and U_2 with increasing P, particularly over both LoS links. Fig. 9 shows the effect of SI coefficients on the outage performance of U_2 where $t = 2$dB. It is observed that the larger v results in the more inferior performance with $P > 0$dB.

In Figs. 10 and 11 where $m_1 = 2, m_2 = 3$, $\Omega_1 = \Omega_2 = 1$, the capacity values in (64) overlap with the simulations. In Fig. 10, there exists the bigger gap between U_1 and U_2 with

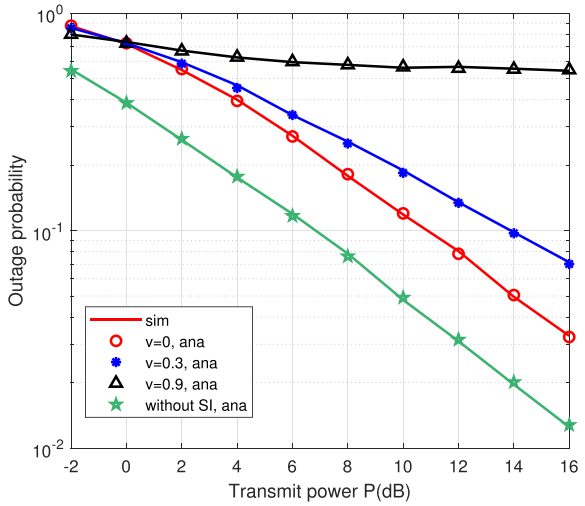

FIGURE 9. Impact of SI coefficients on U_2's outage performance, $N = 2$.

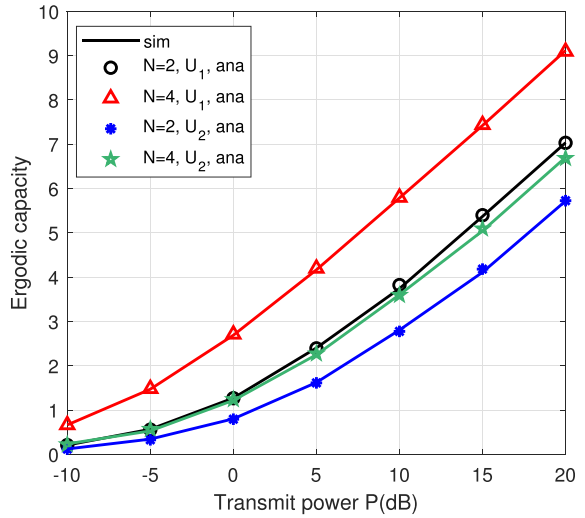

FIGURE 10. Ergodic capacity comparison of U_1 and U_2.

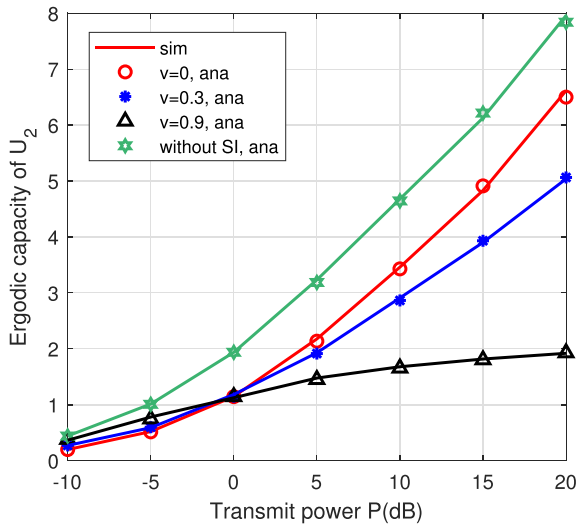

FIGURE 11. Impact of SI coefficients on U_2's ergodic capacity, $N = 4$.

more IRS elements, which implies that the imperfect phases are rather disadvantageous to U_2. Fig. 11 depicts the impact of SI coefficient v on the U_2's ergodic capacity given $t = 2$dB. The SI impact is negligible when $P < 0$dB while the one is conspicuous with the greater v when $P > 0$dB.

VII. CONCLUSION

This paper focuses on the analyses on the OP and EC over Rician and Nakagami fading channels in an IRS-assisted FD IoT or cellular systems, where both reciprocal and non-reciprocal channels are addressed, respectively. For reciprocal channels, where the channels on the same side of the IRS are assumed to be identical, the IRS phase shift design is able to concurrently maximize the received signal energy of both FD users, hence we attach importance to the performance of one FD user due to the system symmetry. In this context, under the hypothetical Gamma distribution with respect to SINR, we have explored the performance of FD users in respective Rician and Nakagami fadings. Simulations reveal that Gamma distribution enables more accurate matching to Nakagami-channel performance. Moreover, We have provided a unified closed form of the EC by utilizing GGL applicable to Rician and Nakagami channels. For non-reciprocal channels where all the channels are distinct, we have presented the accurate OP and EC expressions of both FD users over Nakagami channels. The proposed mathematical framework facilitates the analysis on the effect of various parameters on the IRS-assisted system performance, such as the number of IRS elements, strong line-of-sight components, and self-interference coefficients.

REFERENCES

[1] Q. Wu and R. Zhang, "Towards smart and reconfigurable environment: Intelligent reflecting surface aided wireless network," *IEEE Commun. Mag.*, vol. 58, no. 1, pp. 106–112, Jan. 2020.

[2] S. Abadal, T.-J. Cui, T. Low, and J. Georgiou, "Programmable metamaterials for software-defined electromagnetic control: Circuits, systems, and architectures," *IEEE Trans. Emerg. Sel. Topics Circuits Syst.*, vol. 10, no. 1, pp. 6–19, Mar. 2020.

[3] Q. Wu and R. Zhang, "Intelligent reflecting surface enhanced wireless network via joint active and passive beamforming," *IEEE Trans. Wireless Commun.*, vol. 18, no. 11, pp. 5394–5409, Nov. 2019.

[4] Q. Wu, S. Zhang, B. Zheng, C. You, and R. Zhang, "Intelligent reflecting surface aided wireless communications: A tutorial," *IEEE Trans. Commun.*, vol. 69, no. 5, pp. 3313–3351, May 2021.

[5] P. K. Sharma and P. Garg, "Achieving high data rates through full duplex relaying in multicell environments," *Trans. Emerg. Telecommun. Technol.*, vol. 27, no. 1, pp. 111–121, Jan. 2016.

[6] T.-T. Nguyen, S.Q. Nguyen, P.X. Nguyen, and Y.-H. Kim, "Evaluation of full-duplex SWIPT cooperative NOMA-Based IoT relay networks over nakagami-m fading channels," *Sensors*, vol. 22, no. 5, 2022, Art. no. 1974.

[7] S. Zhang, S. Zhang, F. Gao, J. Ma, and O. A. Dobre, "Deep learning-based RIS channel extrapolation with element-grouping," *IEEE Wireless Commun. Lett.*, vol. 10, no. 12, pp. 2644–2648, Dec. 2021.

[8] C. Huang, R. Mo, and C. Yuen, "Reconfigurable intelligent surface assisted multiuser MISO systems exploiting deep reinforcement learning," *IEEE J. Sel. Areas Commun.*, vol. 38, no. 8, pp. 1839–1850, Aug. 2020.

[9] E. Shi et al., "Wireless energy transfer in RIS-aided cell-free massive MIMO systems: Opportunities and challenges," *IEEE Commun. Mag.*, vol. 60, no. 3, pp. 26–32, Mar. 2022.

[10] X. Mu, Y. Liu, L. Guo, J. Lin, and N. Al-Dhahir, "Exploiting intelligent reflecting surfaces in NOMA networks: Joint beamforming optimization," *IEEE Trans. Wireless Commun.*, vol., 19, no. 10, pp. 6884–6898, Oct. 2020.
[11] Y. Zhang, J. Zhang, M. D. Renzo, H. Xiao, and B. Ai, "Performance analysis of RIS-aided systems with practical phase shift and amplitude response," *IEEE Trans. Veh. Technol.*, vol. 70, no. 5, pp. 4501–4511, May 2021.
[12] A. A. Boulogeorgos and A. Alexiou, "Performance analysis of reconfigurable intelligent surface-assisted wireless systems and comparison with relaying," *IEEE Access*, vol. 8, pp. 94463–94483, 2020.
[13] Q. Tao, J. Wang, and C. Zhong, "Performance analysis of intelligent reflecting surface aided communication systems," *IEEE Commun. Lett.*, vol. 24, no. 11, pp. 2464–2468, Nov. 2020.
[14] I. Yildirim, A. Uyrus, and E. Basar, "Modeling and analysis of reconfigurable intelligent surfaces for indoor and outdoor applications in future wireless networks," *IEEE Trans. Commun.*, vol. 69, no. 2, pp. 1290–1301, Feb. 2021.
[15] A. M. Salhab and M. H. Samuh, "Accurate performance analysis of reconfigurable intelligent surfaces over Rician fading channels," *IEEE Wireless Commun. Lett.*, vol. 10, no. 5, pp. 1051–1055, May 2021.
[16] H. Du, J. Zhang, J. Cheng, and B. Ai, "Millimeter wave communications with reconfigurable intelligent surfaces: Performance analysis and optimization," *IEEE Trans. Commun.*, vol. 69, no. 4, pp. 2752–2768, Apr. 2021.
[17] D. Selimis, K. P. Peppas, G. C. Alexandropoulos, and F. I. Lazarakis, "On the performance analysis of RIS-empowered communications over Nakagami-m fading," *IEEE Commun. Lett.*, vol. 25, no. 7, pp. 2191–2195, Jul. 2021.
[18] Y. Ni, Y. Liu, J. Wang, Q. Wang, H. Zhao, and H. Zhu, "Performance analysis for RIS-assisted D2D communication under Nakagami-*m* fading," *IEEE Trans. Veh. Technol.*, vol. 70, no. 6, pp. 5865–5879, Jun. 2021.
[19] Y. Cheng, K. H. Li, Y. Liu, and K. C. Teh, "Outage performance of downlink IRS-Assisted NOMA systems," in *Proc. IEEE Glob. Commun. Conf.*, 2020, pp. 1–6.
[20] B. Tahir, S. Schwarz, and M. Rupp, "Analysis of uplink IRS-assisted NOMA under Nakagami-m fading via moments matching," *IEEE Wireless Commun. Lett.*, vol. 10, no. 3, pp. 624–628, Mar. 2021.
[21] P. K. Sharma and P. Garg, "Intelligent reflecting surfaces to achieve the full-duplex wireless communication," *IEEE Commun. Lett.*, vol. 25, no. 2, pp. 622–626, Feb. 2021.
[22] B. Lu, R. Wang, and Y. Liu, "Outage probability of intelligent reflecting surface assisted full duplex two-way communications," *IEEE Commun. Lett.*, vol. 26, no. 2, pp. 286–290, Feb. 2022.
[23] S. Atapattu, R. Fan, P. Dharmawansa, G. Wang, J. Evans, and T. A. Tsiftsis, "Reconfigurable intelligent surface assisted two–way communications: Performance analysis and optimization," *IEEE Trans. Commun.*, vol. 68, no. 10, pp. 6552–6567, Oct. 2020.
[24] W. de Souza Jr and T. Abrao, "Outage Performance of RIS-aided Cooperative FD-SWIPT-NOMA in Nakagami-m channels," 2022, *arXiv:2204.01900*.
[25] S. Arzykulov, G. Nauryzbayev, A. Celik, and A. M. Eltawil, "RIS-Assisted full-duplex relay systems," *IEEE Syst. J.*, vol. 16, no. 4, pp. 5729–5740, Dec. 2022, doi: 10.1109/JSYST.2022.3189850.
[26] A. Bhowal and S. Aïssa, "Performance evaluation of RIS-Assisted full-duplex MIMO bidirectional communications with a realistic channel model: (Invited Paper)," in *Proc. Int. Wireless Commun. Mobile Comput.*, 2022, pp. 83–88, doi: 10.1109/IWCMC55113.2022.9824881.
[27] T. N. Nguyen, N. N. Thang, B. C. Nguyen, T. M. Hoang, and P. T. Tran, "Intelligent-reflecting-Surface-Aided bidirectional full-duplex communication system with imperfect self-interference cancellation and hardware impairments," *IEEE Syst. J.*, early access, Apr. 29, 2022, doi: 10.1109/JSYST.2022.3167514.
[28] B. C. Nguyen et al., "Cooperative communications for improving the performance of bidirectional full-duplex system with multiple reconfigurable intelligent surfaces," *IEEE Access*, vol. 9, pp. 134733–134742, 2021.
[29] Z. Peng, T. Li, C. Pan, H. Ren, and J. Wang, "RIS-Aided D2D communications relying on statistical CSI with imperfect hardware," *IEEE Commun. Lett.*, vol. 26, no. 2, pp. 473–477, Feb. 2022.
[30] S. R. Kudumala, A. K. Dubey, P. Gupta, S. Gupta, and E. Sharma, "Hardware impaired RIS assisted multipair FD communication with spatial correlation," *IEEE Commun. Lett.*, vol. 26, no. 9, pp. 2200–2204, Sep. 2022.
[31] A. Papazafeiropoulos, P. Kourtessis, and I. Krikidis, "STAR-RIS assisted full-duplex systems: Impact of correlation and maximization," *IEEE Commun. Lett.*, vol. 26, no. 12, pp. 3004–3008, Dec. 2022, doi: 10.1109/LCOMM.2022.3204893.
[32] Z. Peng, Z. Zhang, C. Pan, L. Li, and A. L. Swindlehurst, "Multiuser full-duplex two-way communications via intelligent reflecting surface," *IEEE Trans. Signal Process.*, vol. 69, pp. 837–851, 2021.
[33] M. Gao, B. Ai, Y. Niu, Z. Han, and Z. Zhong, "IRS-assisted high-speed train communications: Outage probability minimization with statistical CSI," in *Proc. IEEE Int. Conf. Commun.*, 2021, pp. 1–6.
[34] X. Gan, C. Zhong, C. Huang, and Z. Zhang, "RIS-assisted multi-user MISO communications exploiting statistical CSI," *IEEE Trans. Commun.*, vol. 69, no. 10, pp. 6781–6792, Oct. 2021.
[35] S. Atapattu, P. Dharmawansa, M. Di Renzo, C. Tellambura, and J. S. Evans, "Multi-user relay selection for full-duplex radio," *IEEE Trans. Commun.*, vol. 67, no. 2, pp. 955–972, Feb. 2019.
[36] A. Annamalai, C. Tellambura, and J. Matyjas, "A new twist on the generalized marcum Q-function QM(a, b) with fractionaloOrder M. and its applications," in *Proc. 6th IEEE Consum. Commun. Netw. Conf.*, 2009, pp. 1–5.
[37] S. Li, L. Bariah, S. Muhaidat, A. Wang, and J. Liang, "Outage analysis of NOMA-enabled backscatter communications with intelligent reflecting surfaces," *IEEE Internet Things J.*, vol. 9, no. 16, pp. 15390–15400, Aug. 2022.
[38] H. Cohen, *Numerical Approximation Methods*, New York, NY, USA:Springer, 2011.
[39] H. Ghavami and S. Shirvani Moghaddam, "Outage probability of device to device communications underlaying cellular network in suzuki fading channel," *IEEE Commun. Lett.*, vol. 21, no. 5, pp. 1203–1206, May 2017.
[40] H. S. Silva, D. B. T. Almeida, W. J. L. Queiroz, I. E. Fonseca, A. S. R. Oliveira, and F. Madeiro, "Outage probability of the product of two beaulieu–xie, η–μ, κ–μ, or α-μ random variables," *IEEE Antennas Wireless Propag. Lett.*, vol. 19, no. 12, pp. 2182–2186, Dec. 2020.
[41] S. A. Tegos, D. Tyrovolas, P. D. Diamantoulakis, C. K. Liaskos, and G. K. Karagiannidis, "On the distribution of the sum of double-nakagami-m random vectors and application in randomly reconfigurable surfaces," *IEEE Trans. Veh. Technol.*, vol. 71, no. 7, pp. 7297–7307, Jul. 2022.

SUYUE LI received the B.Sc. degree in electrical automation from the Henan University of Science and Technology, Luoyang, China, in 2002, the M.Sc. degree in signal and information processing from the Taiyuan University of Technology, Taiyuan, China, in 2007, and the Ph.D. degree in communication engineering from Shanghai Jiao Tong University, Shanghai, China, in 2013. As a visiting scholar in 2018, she studied with the Department of Electrical and Computer Engineering, University of California, Riverside, CA, USA. She is currently an Associate Professor with the School of Electronics and Information Engineering, Taiyuan University of Science and Technology, Taiyuan. Her main research interests include channel estimation and equalization, MIMO wireless communication, cooperative communication, Massive MIMO, non-orthogonal multiple access, and sparse signal processing.

SEN YAN received the B.Sc. degree in electronic information engineering in 2020 from the Taiyuan University of Science and Technology, Taiyuan, China, where he is currently working toward the M.Sc. degree in electronic information. His research interests include full duplex communications and intelligent reflective surfaces.

LINA BARIAH (Senior Member, IEEE) received the M.Sc. and Ph.D. degrees in communications engineering from Khalifa University, Abu Dhabi, UAE, in 2015 and 2018, respectively. She was a Visiting Researcher with the Department of Systems and Computer Engineering, Carleton University, Ottawa, ON, Canada, in 2019. She is currently a Postdoctoral Fellow with the KU Center for Cyber-Physical Systems, Khalifa University, and an Affiliate Research Fellow, James Watt School of Engineering, University of Glasgow, Glasgow, U.K. Her research interests include advanced digital signal processing techniques for communications, machine learning, cooperative communications, non-orthogonal multiple access, cognitive radios, reconfigurable intelligent surfaces, aerial networks, and visible light communications. Dr. Bariah was a Member of the technical program committee of a number of IEEE conferences, such as ICC and Globecom. She is currently an Associate Editor for the IEEE OPEN JOURNAL OF THE COMMUNICATIONS SOCIETY and the Area Editor of *Physical Communication (Elsevier)*. She is the Guest Editor of *RS Open Journal on Innovative Communication Technologies*. She is the Session Chair and an Active Reviewer for numerous IEEE conferences and journals.

SAMI MUHAIDAT (Senior Member, IEEE) received the Ph.D. degree in electrical and computer engineering from the University of Waterloo, Waterloo, ON, Canada, in 2006. From 2007 to 2008, he was an NSERC Postdoctoral Fellow with the Department of Electrical and Computer Engineering, University of Toronto, Toronto, ON, Canada. From 2008 to 2012, he was an Assistant Professor with the School of Engineering Science, Simon Fraser University, Burnaby, BC, Canada. He is currently a Professor with Khalifa University, Abu Dhabi, UAE, and an Adjunct Professor with the Department of Systems and Computer Engineering, Carleton University, Ottawa, ON, Canada. His research interests include wireless communications, optical communications, IoT with emphasis on battery-less devices, and machine learning. He is currently the Area Editor of the IEEE TRANSACTIONS ON COMMUNICATIONS and Lead Guest Editor of the IEEE OJ-COMS LARGE-SCALE WIRELESS POWERED NETWORKS WITH BACKSCATTER COMMUNICATIONS special issue. He was the Senior Editor and Editor of the IEEE COMMUNICATIONS LETTERS and IEEE TRANSACTIONS ON COMMUNICATIONS, and an Associate Editor for the IEEE TRANSACTIONS ON VEHICULAR TECHNOLOGY.

ANHONG WANG received the B.S. and M.S. degrees from the Taiyuan University of Science and Technology, China respectively in 1994 and 2002, and the Ph.D. degree with the Institute of Information Science, Beijing Jiaotong University,Beijing, China, in 2009. She became an Associate Professor with TYUST in 2005 and became a Professor in 2009. She is currently the Director of Institute of Digital Media and Communication, Taiyuan University of Science and Technology, Taiyuan, China. Her research interests include image and video coding and secret image sharing, etc.